

Three-dimensional elastic earthquake modelling based on integrated seismological and InSAR data: the $M_w = 7.2$ Nuweiba earthquake, gulf of Elat/Aqaba 1995 November

G. Shamir,¹ G. Baer² and A. Hofstetter¹

¹Geophysical Institute of Israel, Lod, Israel. E-mail: gadi@jprg.energy.gov.il

²Geological Survey of Israel, Jerusalem, Israel. E-mail: baer@mail.gsi.gov.il

Accepted 2003 March 10. Received 2002 October 11; in original form 2001 December 28

SUMMARY

The Nuweiba earthquake (1995 November 22; $M_w = 7.2$), the largest seismic event along the Dead Sea Transform (DST) in at least 160 yr, ruptured 45–50 km along the Aragonese segment of the left-stepping strike-slip fault system occupying the gulf of Elat/Aqaba (southern segment of the DST). The rupture initiated in a partly normal, low-slip first subevent near the southern end of the fault and propagated unilaterally north-northeastward as a high-slip, nearly pure sinistral second subevent, which was responsible for over 90 per cent of the total seismic moment. The source mechanism and slip distribution, derived from inversion of teleseismic broad-band waveforms, are used to construct a 3-D elastic model of the earthquake based on the boundary elements method, resulting in the full 3-D displacement and stress fields induced by the earthquake. In the absence of sufficient Global Positioning System data, the only other constraints on the geometry and slip distribution of the rupture are provided by interferometric synthetic aperture radar (InSAR) measurements spanning the coseismic and early post-seismic period. We calculate simulated interferograms by transforming the calculated surface displacement field into the satellite coordinate system and comparing them with the observed interferograms. The model parameters are then iteratively modified until a best-fitting model is obtained, providing a refined set of static source parameters for the mainshock. This model is then used to calculate the static Coulomb stress changes induced by the mainshock on the step-over faults, suggesting that the major ($M_w \geq 5$) aftershocks in the first eight post-seismic months were triggered by small changes (<1 bar) in the left-lateral Coulomb stress, with effective friction coefficient not higher than 0.2. Aftershock distribution and mechanisms indicate that the available Coulomb stress dropped below the frictional strength of the fault but was not complete.

Key words: Dead Sea transform, earthquakes, elastodynamics, gulf of Elat/Aqaba, stress distribution.

1 INTRODUCTION

The Nuweiba earthquake ($M_w = 7.2$; 1995 November 22) ruptured along the Aragonese fault, a major segment of the Dead Sea transform (DST) in the gulf of Elat/Aqaba (Fig. 1). It was the largest earthquake to occur along the DST in at least 160 yr, and was strongly felt in Egypt, Israel, Jordan and Saudi Arabia. The earthquake was associated with substantial ground shaking, causing minor damage to population centres, widespread rock falls in eastern Sinai and unusually high ground accelerations (Gitterman *et al.* 1996). It demonstrated the potential of the DST for large destructive earthquakes, as suggested by historical records from the Middle East.

The gulf of Elat/Aqaba is the inner, active part of the 60–80 km wide deformation zone constituting the southern segment of the Dead Sea Transform (Eyal *et al.* 1981) (Fig. 1). This transform

connects the Red Sea spreading centre in the south, through the Dead Sea rift, to the Taurus–Zagros collision zone in the north. The total strike-slip offset along this boundary is approximately 105 km (Quennell 1959; Freund *et al.* 1970; Bartov 1974; Garfunkel *et al.* 1981; Hatcher *et al.* 1981), of which at least 30 km probably took place since the Miocene (Joffe & Garfunkel 1987). The gulf itself is approximately 180 km long, 15–25 km wide and reaches a maximum depth of 1850 m in its central basin (Allan *et al.* 1964; Drake & Girdler 1964; Ben-Avraham *et al.* 1979a). The gulf has been the seismically most active segment of the DST plate boundary since instrumental monitoring initiated in the region in the early 1980s. West of the gulf, in eastern Sinai, the plate boundary deformation zone consists of a system of Neogene strike-slip faults, which have a total left lateral offset of 24 km (Bartov *et al.* 1980; Eyal *et al.* 1981). The gulf is bordered by coastal normal faults, which probably ceased

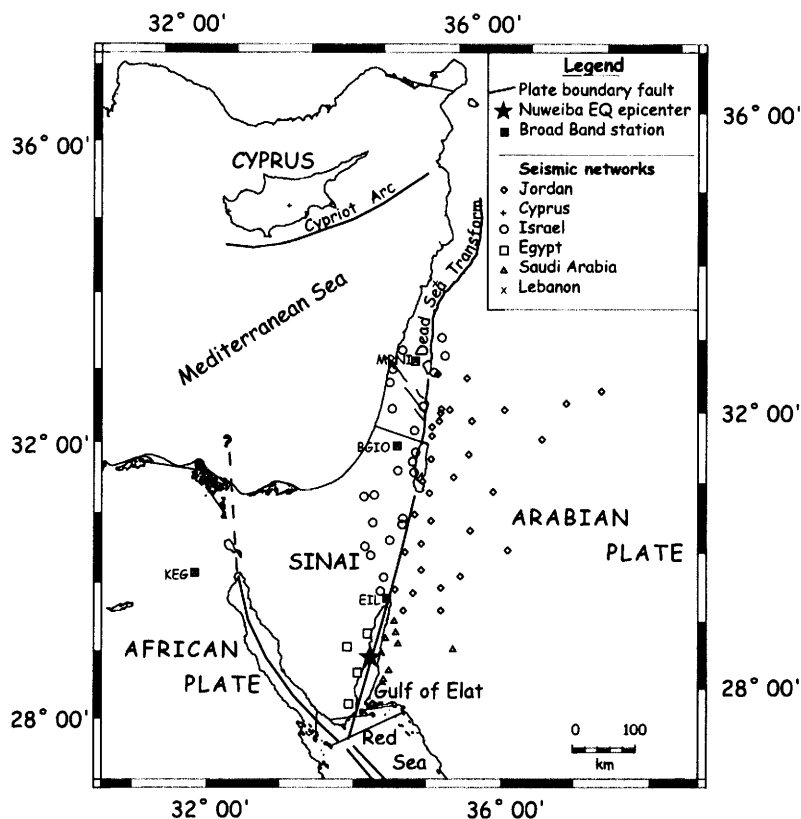


Figure 1. Location map, also showing regional seismic networks in the southern Dead Sea Transform region.

to operate prior to the formation of the current inner-gulf strike-slip system (Eyal 1973; Eyal *et al.* 1981).

Geophysical surveys of the gulf of Elat/Aqaba have taken place since the late 1970s and include echo sounding, seismic profiles, coring and measurements of gravity, magnetics and heat flow (Ben-Avraham *et al.* 1978, 1979a,b; Hall & Ben-Avraham 1978; Ben-Avraham 1985; Ben-Avraham & Tibor 1993). The gulf bathymetry (Fig. 2) is generally asymmetrical in E–W profiles, usually with steep eastern slopes and devoid of continental shelves. The gulf floor is occupied by several elongated, fault-bounded distinct basins striking NNE. The basins are filled with discontinuous and steeply inclined sedimentary layers, indicating syntectonic sedimentation at spatially varying rates. The gulf narrows to a mere single canyon at 29° N, at the transition between the shallow, flat-bottomed northern Elat basin and the deep, warped-bottom, Aragonese basin (Ben-Avraham 1985). Thus, in the central basin the rate of subsidence relative to the rate of sedimentation is presumably higher than in the northern basin. The southern basin occupies the eastern half of the gulf and contains two local depo-centres (Dakar and Tiran) deformed in a manner similar to that of Aragonese basin. The major faults of the gulf (Fig. 2) are arranged en echelon, with transverse, probably normal faults at basin ends and interiors. The basins are therefore the product of extension at the step zones between the major left-stepping strike-slip faults (Ben-Avraham *et al.* 1979a). This is consistent with the geological left-lateral offset along this plate boundary. Seismic reflection profiles (Ginzburg *et al.* 1979) show southward crustal thinning in the gulf, from 35 to 27 km, with the sharpest transition under the Aragonese basin. On this basis, Mart (1982) and Ben-Avraham (1985) suggested that this thinning, and

transition in other geophysical properties, might reflect northward rift propagation along the gulf.

Since the early 1980s, the gulf region was affected by a number of earthquake swarms (El Isa *et al.* 1984; Alamri 1991; Shamir & Shapira 1994). The 1983 and 1990–91 sequences (with peak magnitudes $M_L = 5.2$ and 4.3, respectively) were mostly confined to the Elat basin, and are therefore attributed to the Elat/Aragonese fault step zone. The 1993 sequence (peak magnitudes $M_L = 5.8$ and 5.6) occurred primarily in and around the Aragonese basin, i.e. in the Aragonese/Arnona fault step zone. Thus, the seismicity in the gulf of Elat in the 12 yr prior to 1995 was clustered in space and time, with the release of seismic energy mostly being localized at the two major fault step zones. No similar activity was reported for the gulf over previous decades (the regional catalogue is considered complete for $M_L \geq 4.8$ since 1900 and for $M_L \geq 4.0$ since 1940).

Instrumental seismic monitoring of the gulf of Elat initiated in the early 1980s. As a result of the distribution of seismic networks around the gulf (Fig. 1), accurate epicentre determination requires integration and synchronization of data from several sources and occasionally suffers from poor station coverage, incomplete or unpublished bulletins and a short recording history. When integrating data from the Israel and Jordan networks, as has been routinely done since 1996, location errors of up to a few kilometres may be obtained for the northern and central gulf.

In this paper we integrate seismological and interferometric synthetic aperture radar (InSAR) observations in order to constrain a 3-D mechanical model of the Nuweiba earthquake. The model serves to refine previous geodetic and seismological estimates of

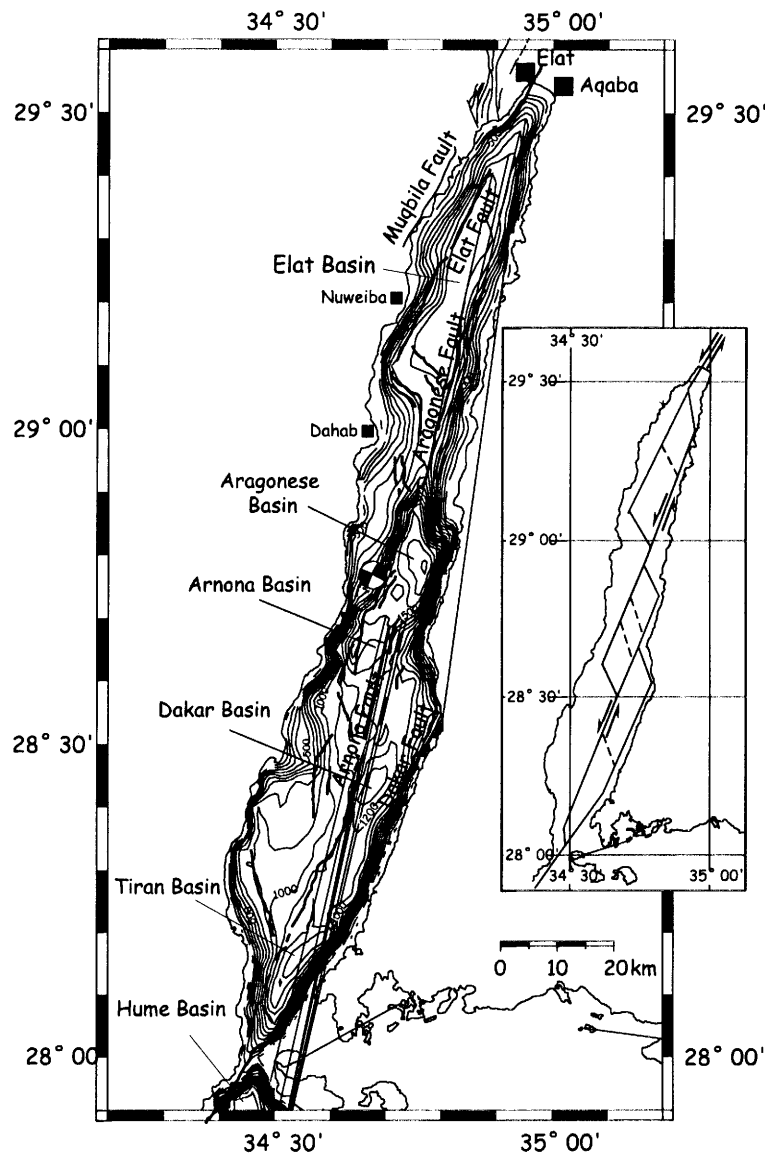


Figure 2. Bathymetry, mapped faults and schematic fault structure (inset) of the gulf of Elat/Aqaba (after Hall & Ben-Avraham 1978; Ben-Avraham *et al.* 1979a; Ben-Avraham 1985; Ben-Avraham & Tibor 1993).

the mainshock source mechanism. It is then used to calculate the Coulomb stress changes induced by the Nuweiba earthquake onto the neighbouring step-over faults, triggering a number of $M \geq 5$ aftershocks.

2 SEISMOLOGICAL OBSERVATIONS

The Nuweiba earthquake occurred on 1995 November 22 at 04:15 GMT and measured $M_L = 6.2$ on the local magnitude scale based on coda duration and $M_w = 7.2$ on the moment magnitude scale. Based on short-period data from Israel, Jordan, Saudi Arabia, Cyprus and Egypt, the epicentre was at 28.76°N , 34.66°E (Fig. 2) and the hypocentral depth was approximately 13 km. To solve for the source mechanism and moment distribution, Hofstetter *et al.* (2003) inverted teleseismic broad-band waveforms of the Nuweiba earthquake using a method similar to that of Hartzell & Heaton (1986).

The data used was from stations at epicentral distances between 30° and 90° , obtained from the IRIS and GEOSCOPE data centres. The complex waveforms suggest that the mainshock consisted of two major episodes of energy release (Fig. 3a), with the source parameters listed in Table 1.

The first subevent, with a larger normal component, is consistent with the P -wave first-motion focal plane solution (calculated using the code of Reasenber & Oppenheimer 1985), based on local and regional observations with exceptionally good (for this region) azimuthal distribution (Fig. 3b). The second subevent is dominantly left-lateral and produced over 90 per cent of the seismic moment. Other inversion solutions for the Nuweiba mainshock suggested seismic moments of 5.8×10^{19} N m (Kikuchi 1995), 7.2×10^{19} N m (Harvard CMT), 4.9×10^{19} N m (NEIC), 3.8×10^{19} N m (Pinar & Turkelli 1997) and 7.42×10^{19} N m (Klinger *et al.* 1999). All previous analyses resulted in similar overall left lateral

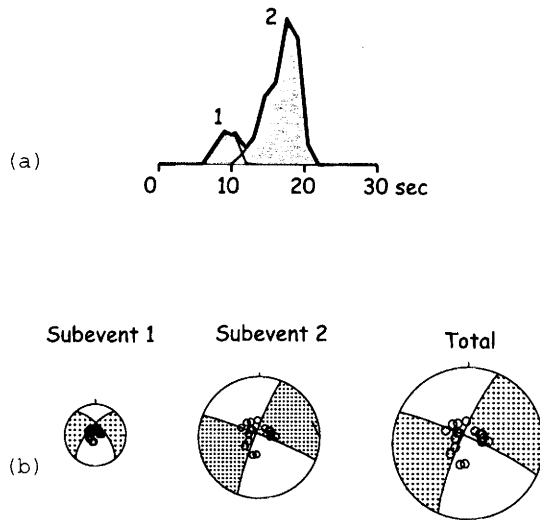


Figure 3. Source time function (a) and mechanism (b) of the Nuweiba earthquake based on inversion of regional broad-band data (Hofstetter *et al.* 2003).

mechanisms. Pinar & Turkelli (1997) emphasized the proximity and similarity of mechanism (also shown by Fattah *et al.* 1997) between the first subevent and a 1993 $M_s = 6.1$ normal event. Klinger *et al.* (1999) performed a body wave inversion and suggested that the earthquake consisted of three subevents on three distinct faults. As noted by Klinger *et al.* (2000) and discussed below, this is not supported by the InSAR data.

The Nuweiba mainshock rupture had a strong NNE directivity effect, with the narrowest pulse directed in about azimuth 10° and the widest in 190° (R. Katzman, Pers. comm., 1995; Kikuchi 1995; Fig. 4). It therefore nucleated near the southern end of the Aragonese fault and propagated unilaterally to the NNE, in accordance with the known fault structure in the gulf of Elat (Fig. 2; Ben-Avraham *et al.* 1979a; Ben-Avraham 1985).

Using the moment distribution obtained from the teleseismic waveform (H-K. Thio, Pers. comm, 2000; Hofstetter *et al.* 2003) and rigidity layering based on the velocity structure in the region (Table 2), we derived the mainshock slip distribution (Fig. 5). Taking into account the unilateral rupture propagation, the slip distribution shows that the maximal slip zone became shallower as the rupture propagated northward and changed from partly normal to mostly strike slip. The inversion also allows for rake variation, which in this case is reasonably constrained only in the epicentral and in the high-slip region of the second subevent.

3 IN SAR OBSERVATIONS

Next we impose independent geodetic constrains on the estimate of the static source parameters. The Global Positioning System (GPS)

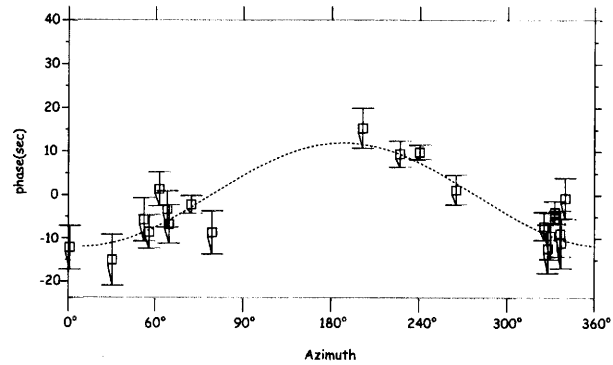


Figure 4. Azimuthal change of phase length, indicating directivity of the Nuweiba earthquake rupture to the NNE (Katzman, Pers. comm., 1996; Kikuchi 1995).

Table 2. Velocity and rigidity structure (based on Feigin & Shapira 1994).

Depth (km)	V_p (m s ⁻¹)	V_s (m s ⁻¹)	Density (kg m ⁻³)	Rigidity (N m ⁻²)
1-7.2	5510	3100	2600	2.5E+10
7.2-21.64	6230	3600	2800	3.63E+10
21.64-	7950	4450	3200	6.3E+10

and interferometric synthetic aperture radar (InSAR), that are space-referenced geodetic techniques that provide displacement measurements with subcentimetre accuracy and enable the determination of deformation rates and patterns over broader areas, and considerably shorter time intervals than previously possible. InSAR has been shown to be particularly effective for mapping earthquake displacement fields in the co-seismic and post-seismic phases (e.g. for the Landers earthquake; Massonnet & Feigl 1998, and references therein) and for estimating post-seismic strain relaxation times (e.g. Peltzer *et al.* 1996).

Sporadic GPS data from the gulf region show southward displacement of the city of Elat (100 km north of the epicentre) by 18.1 ± 1.2 mm with respect to Bar-Giora (350 km north of the epicentre; Bechor 1998) and coseismic displacement of 166 mm in a direction of 246° in Dahab (eastern Sinai, 26 km southwest of the epicentre; Kimata *et al.* 1997). Given these scarce GPS data and the lack of surface observations (the entire rupture trace was submarine), InSAR observations of the coseismic surface deformation provide the only non-seismological constraints on the static parameters of the Nuweiba earthquake (Baer *et al.* 1999, 2001). In this study we used SAR data collected by the ERS-1 satellite, which imaged the area between 1993 January and 1996 May, and the ERS-2 satellite, which has been imaging the area since 1995 July. The SAR operates in the C-band at a wavelength of 56.5 mm, with a normal orbital cycle of 35 d for each satellite. During the overlapping period (1995-1996), the satellites performed tandem missions at 1 d

Table 1. Static source parameters as derived from inversion of teleseismic data (Hofstetter *et al.* 2002).

Sub-event	Source epicentre	Length (km)	Depth (km)	Strike	Dip	Rake	Moment ($\times 10^{19}$ N m)
1	28:76 N, 34:66 E		15 ± 1	295 ± 5	60 ± 2	-20 ± 5	0.6 ± 0.03
2			10 ± 1	202 ± 5	77 ± 2	-15 ± 5	7.1 ± 0.1
Overall		60	13 ± 1	205 ± 5	75 ± 2	-17 ± 5	7.7 ± 0.08

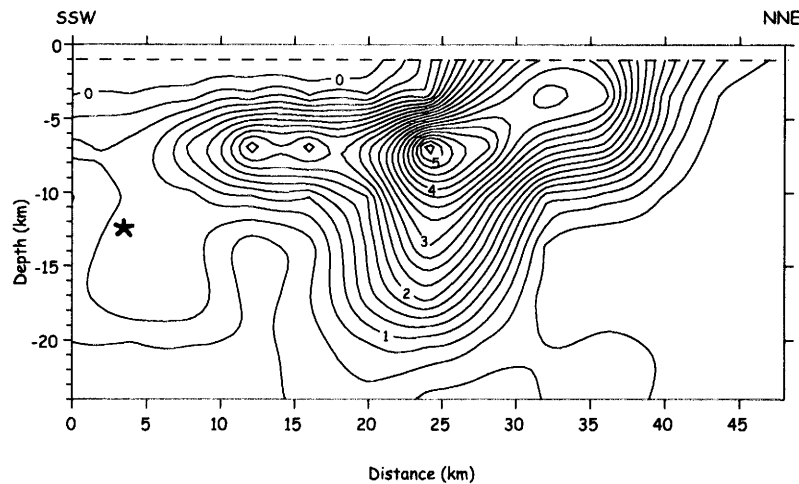


Figure 5. Slip distribution of the Nuweiba mainshock based on the moment distribution obtained from waveform inversion (H.-K. Thio, Pers. comm., 2000; Hofstetter *et al.* 2003). The slip values are those of the final elastic model, described in the text and summarized in Table 3).

intervals. The selected SAR scenes (frames 567 and 585 of the northward track) are approximately $100 \times 100 \text{ km}^2$ each (Fig. 6). To isolate the phase change due to ground displacements from the topographic phase, the latter is removed. This is done by projecting a digital elevation model (DEM) into the radar coordinates and removing it from the full-resolution interferogram. Because no detailed DEM is available for the entire study area we use the low-resolution USGS-developed GTOPO30 DEM, with a horizontal grid spacing of 30 arcsec (approximately 1 km). To generate a coseismic interferogram we chose orbits ERS2-02201 (1995 September 21) and ERS2-19235 (1998 December 24). This pair has only been analysed previously by Baer *et al.* (2001). Its major advantages are the continuity between the two frames, the absence of orbital errors and the short perpendicular baseline (8 m), which allows the use of the low-resolution DEM to remove the topographic fringes. In addition to removing the crude DEM, the residual phase from a suitable Tandem ERS-1 to ERS-2 pair is unwrapped and added back to the crude topographic phase model to form a full-resolution topography model needed for isolating the phase signal due to ground motion. The coseismic interference fringes represent displacement along the satellite line-of-sight (LOS) direction, with each fringe cycle corresponding to 2.8 cm of movement. A relatively high fringe rate is observed in the northwestern quadrant, where the LOS displacement reaches an extension of $\sim 22.5 \text{ cm}$ relative to an arbitrary reference fringe marked F_r . The northeastern quadrant reaches approximately 6.5 cm of LOS extension and the southeastern quadrant approximately the same amount of LOS shortening. Thus the northern quadrants moved away, and the southern moved towards the satellite, due to the coseismic displacements. As shown by Baer *et al.* (2001), the effect of post-seismic deformation on these images was minor and localized.

4 ELASTIC MODELLING

Based on the seismological data, we construct an initial elastic mechanical model of the Nuweiba earthquake, in order to: (1) refine the source parameter estimation; (2) calculate simulated interferograms based on detailed numerical modelling; and (3) estimate the Coulomb stress changes on the step-over faults, particularly

in the northern, more populated part of the gulf. We utilize a 3-D numerical algorithm (BEASY, Computational Mechanics, UK; Trevelyan *et al.* 1995), which is based on the elastic boundary element method (BEM). In this algorithm, an integral equation describes the behaviour of the model under some loading. For each boundary element, a known fundamental solution relates the displacements and tractions occurring when a point force is applied. The contribution of a single-element solution to the tractions and displacements elsewhere on the surface of the model is obtained by integrating this Green's function over the boundary. By setting such an integral equation for each of the N elements defining the boundary, a system of N equations is set for each of the N elements defining the boundary. The system of equations can be solved for the displacement and traction vectors when appropriate boundary conditions are applied to all elements. An important advantage of such BEM models is that integration is performed only over the boundaries (external and internal) and therefore only they must be discretized. This algorithm was previously applied to faulting problems by Katzman *et al.* (1995) and tenBrink *et al.* (1996), who also discussed its accuracy in comparison with analytical dislocation solutions.

The geometry and boundary conditions of the BEM model for the Nuweiba earthquake are shown in Fig. 7, based on the fault structure in the gulf of Elat/Aqaba (Ben-Avraham *et al.* 1979a,b; Ben-Avraham 1985, Fig. 2) and eastern Sinai (Eyal 1973; Hildebrand *et al.* 1974). The initial boundary conditions are the source dimensions and the slip distribution (in a discretized form) derived from the inversion of teleseismic P and SH waveforms for this event (H.-K. Thio, Pers. comm., 2000; Hofstetter *et al.* 2003; Figs 5 and 7). We calculate the 3-D surface displacement field in the Earth-based coordinate system, and derive the components in the satellite-based system by standard coordinate transformation. The component along the Earth-to-satellite line of sight is then 'wrapped' in cycles of 2.8 cm to produce simulated interferograms comparable with the observed interferogram of Fig. 6.

The lobe distribution in our preliminary results showed that the surface area of the rupture patch was overestimated by the seismological solution by approximately 10–15 per cent. In our final models the rupture is mostly enclosed in a $48 \times 25 \text{ km}^2$ patch consisting of 13×7 discrete elements, approximately

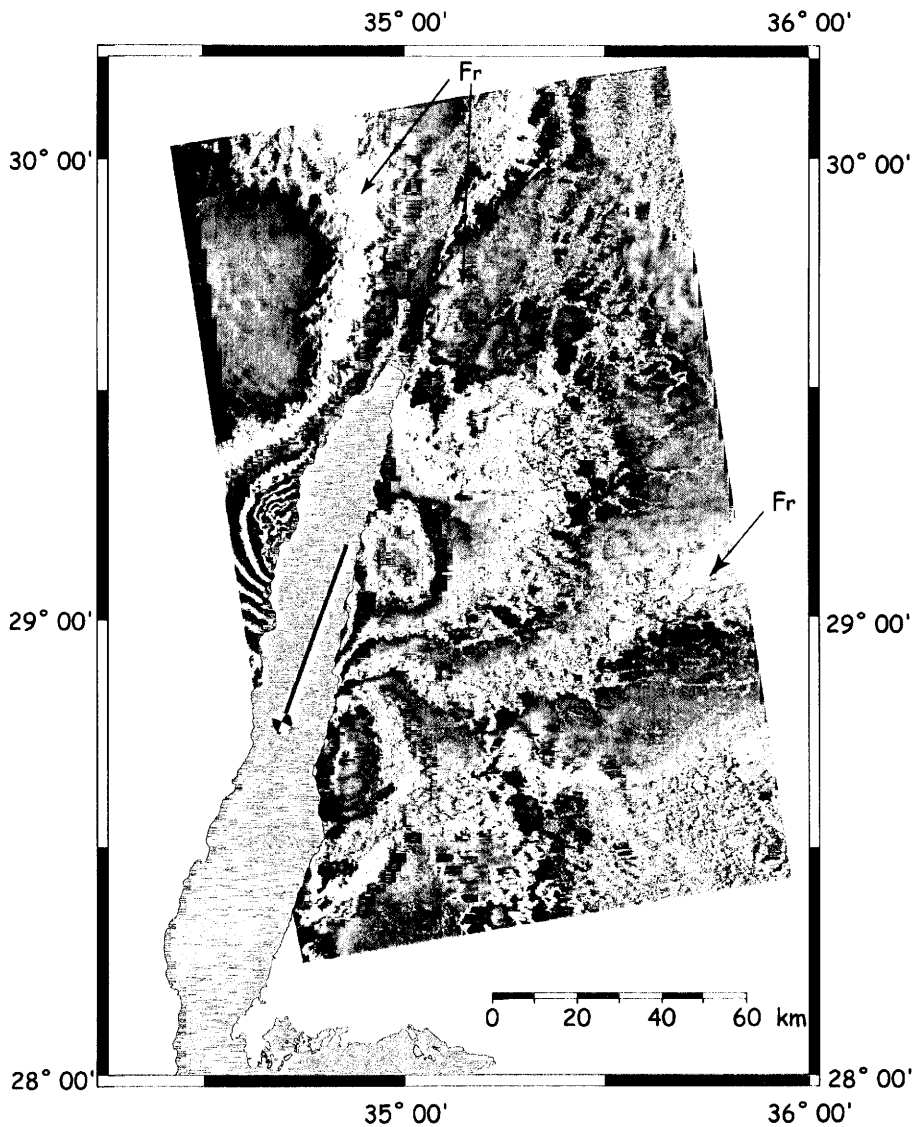


Figure 6. Cosismic interferogram of frames 567 and 585 for the period 1995 September 21 to 1998 December 24. Each fringe cycle corresponds to 2.8 cm of satellite-to-ground line-of-sight displacement. Based on the colour order, the two northern lobes reflect extension of the LOS component and the two southern lobes reflect shortening. A reference fringe marked F_r shows that the extension reaches ~ 22.5 and ~ 6.5 cm in the NW and NE lobes, respectively. The fault trace is the overall upward projection of the slip patch, not the surface rupture.

$3.7 \times 3.4 \text{ km}^2$ each (Fig. 7). The shallowest extent of the rupture is at 1 km depth, the mean water depth along the Aragonese fault. The model is rigidity-layered (see inset in Fig. 7), based on a layered model of the crust in Israel (table 2, after Feigin & Shapira 1994). The model is relevant to the mainshock near field (approximately one to two rupture lengths away from the rupture patch), where both static stress changes and transient effects (e.g. pore pressure changes and seismic waves) contribute to triggering of aftershocks and to time delays or advances of earthquakes on neighbouring faults (Gomberg *et al.* 1998).

Next, we modified the slip and rake distribution in order to improve the consistency between the real and simulated distribution and the rate of fringes. The main modifications were the introduction of smooth slip gradients at the edges of the slipped area, a smooth

interpolation between zones of reasonably constrained rake values and iterative small variations in the slip rake. This resulted in an overall reduction of over 20 per cent in the slip values compared with those derived from the waveform inversion, and rake variations between 35° (in the epicentral area) and 12° (in the high slip zone of the second subevent). An overall rupture length of L-48 km is consistent with the average shear wave velocity of 3.5 km s^{-1} typical for that region (Ginzburg *et al.* 1979; Barazangi *et al.* 1996), a rupture velocity that is 85 per cent of the shear wave velocity, and the overall event duration of 16 s. The mean down-dip width is $w=24 \text{ km}$. The total seismic moment is obtained by summing up the moment contribution from all 91 elements (not all slipped) in the final model,

$$M_0 = \sum M_i = a \sum \mu_i u_i = 7.0 \times 10^{19} \text{ N m}, \quad (1)$$

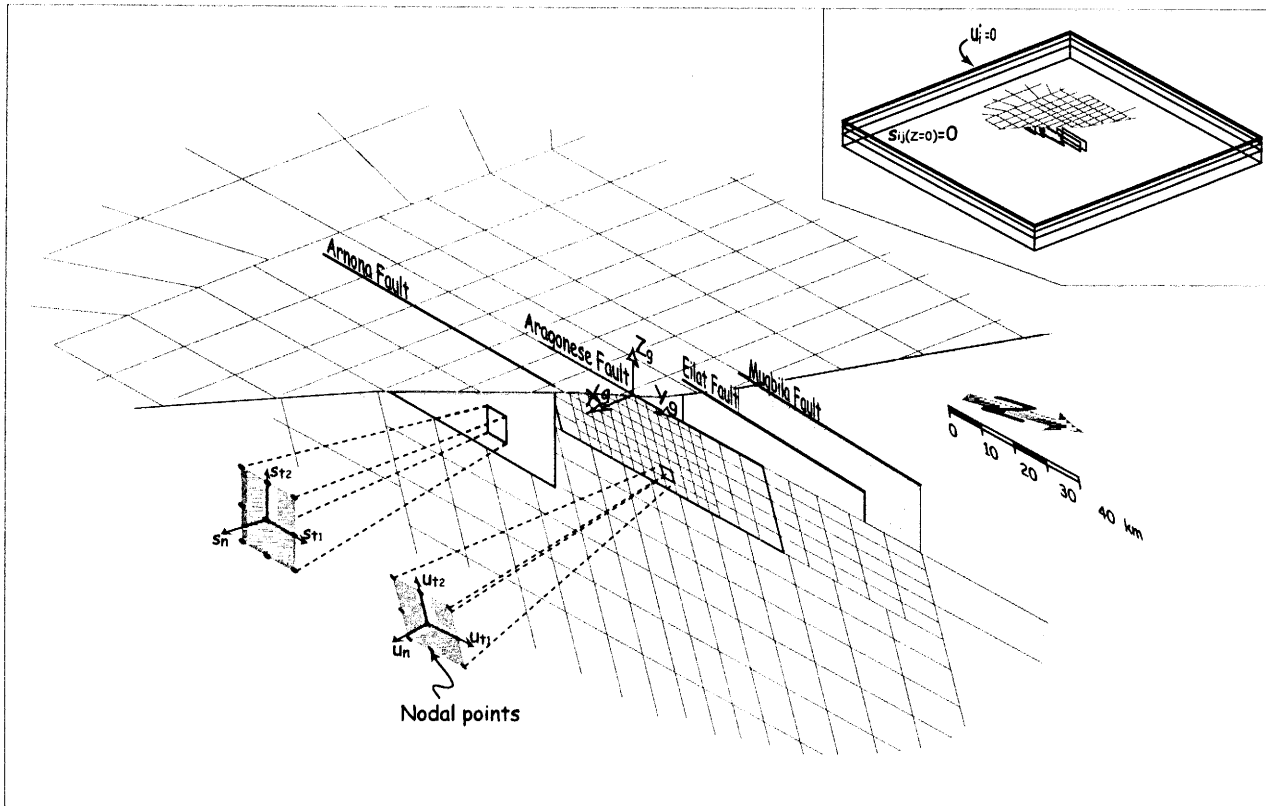


Figure 7. Elastic model of the Nuweiba earthquake. The model is embedded in a 100 × 100 km horizontally layered crustal block with downward increasing rigidity (see inset and Table 2). Internal and external boundaries are meshed with quadratic elements (nine nodal points each). Displacements vanish at the remote edges of the model, and stresses vanish at its upper boundary to simulate the earth surface. Slip boundary conditions, $u_i (i = t_1, t_2, n)$, reflect the discretized form of the slip distribution (Fig. 5) on the Aragonese fault patch. $s_i (i = t_1, t_2, n)$ are the stress components resolved onto the neighbouring faults.

where a is the constant element area, and u_i and μ_i are the slip and rigidity values, respectively, of the i th element. The resulting mean stress drop is (Kanamori & Anderson 1975)

$$\overline{\Delta\tau} = \frac{2}{\pi} \frac{M_0}{w^2 L} = 5.06 \text{ MPa.} \quad (2)$$

The simulated interferogram derived from the final best-fitting earthquake model is shown in Fig. 8. The overall geometry and magnitude of the modelled strain pattern are in good agreement with the observed interferogram. This is particularly so in the northern lobes, representing the second, major subevent. The small inconsistency in the orientation and magnitude of the southeastern lobe may be the result of the particular slip vector rake distribution in the first subevent. The final parameters of the modelled fault patch are summarized in Table 3. Note, however, that unlike in dislocation models, the modelled rectangle is not equivalent to the slip patch but only gives a general notion of the size of the fault. Furthermore, note in Figs 5 and 9 that the rupture seems to have reached the surface (i.e. the gulf bottom) only over the NE half of the fault. This illustrates the potential underestimation of earthquake magnitudes when derived from their surface rupture length.

5 COULOMB STRESS CHANGES AND AFTERSHOCK DISTRIBUTION

The final best-fitting model of the Nuweiba earthquake is used to calculate the changes in the 3-D elastic fields, particularly the changes in the left-lateral Coulomb failure stress, $\Delta\tau_f = \Delta\tau_{LL} + \mu_{\text{eff}} \cdot \Delta\sigma_n$, induced onto the step-over faults. For each fault, $\Delta\tau_{LL}$ is the change in left lateral shear stress, $\Delta\sigma_n$ is the change in normal stress and μ_{eff} is the effective friction coefficient, which accounts for pore pressure effects. The regional stress tensor can be regarded as a constant at the seismological timescale and controls the absolute stress level but not the earthquake-induced stress change. Since no quantitative data on the regional state of stress in this region is available, we limit our analysis to this stress change. In Fig. 9 the Coulomb stress changes on the step-over faults are plotted along with the slip and rake distribution on the Aragonese fault. Also shown are the hypocentres and dates of three major ($M_w \geq 5$) left-lateral aftershocks. The effect of increasing the effective friction coefficient on the Arnona fault is to deepen the zone of positive Coulomb stress change near the northern edge of this fault. Since the $M_w = 5.2$ aftershock occurred further south, we conclude that this shallow high-stress zone did not reach the depth of the hypocentre (approximately 9 km), which constrains the effective friction coefficient to be less than 0.2. As expected, the areas of

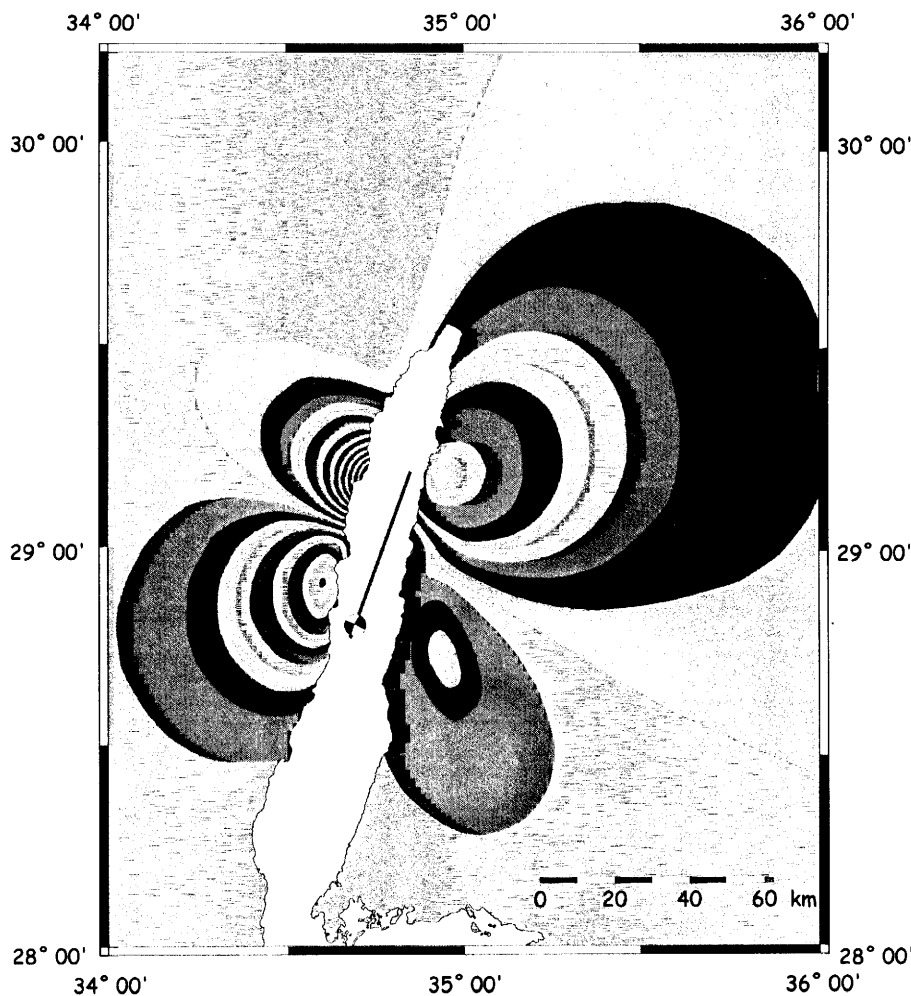


Figure 8. Simulated interferogram of the co-seismic LOS surface displacement of the Nuweiba earthquake, based on the elastic model shown in Fig. 7. The inclined rectangle marks the limit of the observed data (Fig. 6). Each fringe (colour cycle) represents 2.8 cm displacement along the LOS direction. The fault trace is the overall upward projection of the slip patch.

increased LL Coulomb stress lie beyond the overlap zones of the mainshock rupture. All three aftershocks seem to have been triggered by extremely small Coulomb stress increases (0.01–0.02 MPa), similar to what was reported in other cases (e.g. King *et al.* 1994). It should be noted that the $M_w \geq 5.6$ aftershock northwest of the mainshock did not occur on the first step-over fault (Elat fault) but rather on the more distant one (Muqbila fault). Geomor-

phic evidence along the latter (Bowman & Gerson 1986) suggests that it was active during Holocene times, and InSAR data indicates that it actually slipped during or immediately after the Nuweiba earthquake (Baer *et al.* 2001).

The overall distribution of 177 aftershocks of the Nuweiba earthquake in the magnitude range $3.5 \leq M_w \leq 7.2$ are shown in Fig. 10. These aftershocks were recorded by the Israel Seismic Network (ISN) over the 8 months following the mainshock. For 58 aftershocks with $M_w \geq 4$, the broad-band seismograms of BGIO (ISN) and KEG (MEDNET) were used by Hofstetter *et al.* (2003) to obtain the moment and source mechanism by the method of Dreger & Helmberger (1993). Stress drop values were calculated from short-period and broad-band seismograms. Unlike the case of the larger ($M_w \geq 5$) aftershocks, no simple correlation can be found between this distribution and the static Coulomb stress change. Nevertheless, it should be noted that aftershocks, in particular left-lateral events, are completely absent along the mainshock rupture segment. They cluster beyond and off its ends, in the Elat basin to the north and the Arnona basin to the south. A distinct cluster of NW-trending normal-faulting aftershocks occurred along an elongated

Table 3. Final model parameters.

Rupture patch:	
Overall size	$48 \times 14 \text{ km}^2$
NNE corner	29.17 N/34.86 E
SSW corner	28.78 N/34.68 E
Strike	200°
Dip	80
Slip vector:	
Rake	variable, 12° – 35°
magnitude	variable (Figs 5 and 9)
Moment	$7.0 \times 10^{19} \text{ Nm}$
Stress drop	5.06 MPa

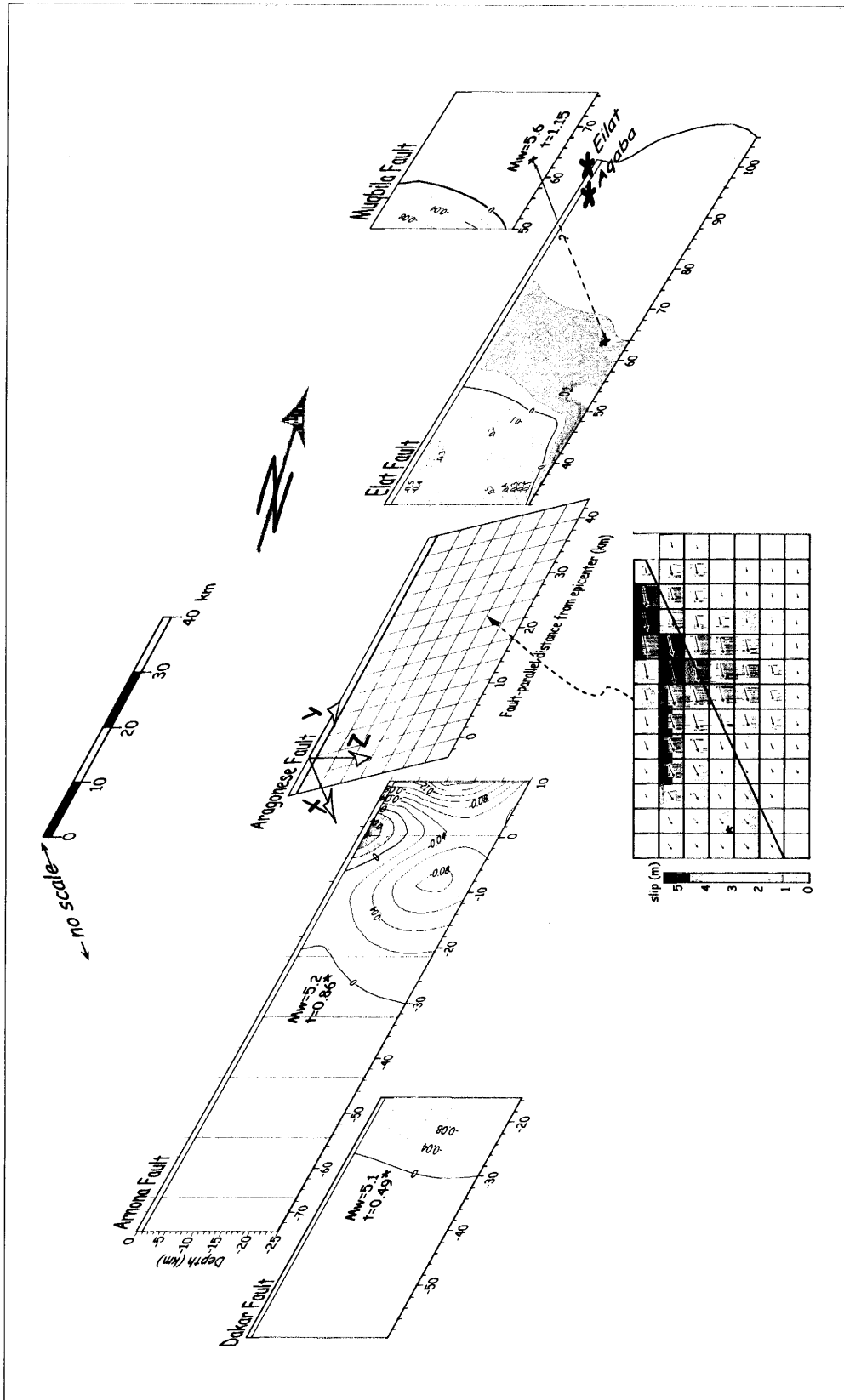


Figure 9. Left lateral Coulomb stress change on the fault segments to the north (Eilat and Mudqibla) and to the south (Armona and Dakar) of the ruptured Aragonese fault, induced by the Nuweiba earthquake. The calculation is based on the elastic model shown in Fig. 7, and the discretized form of the slip and rake distribution on the Aragonese fault. Also shown are the hypocentres and time of occurrence (in days after the mainshock) of the three $M_w \geq 5$ aftershocks on the step-over faults.

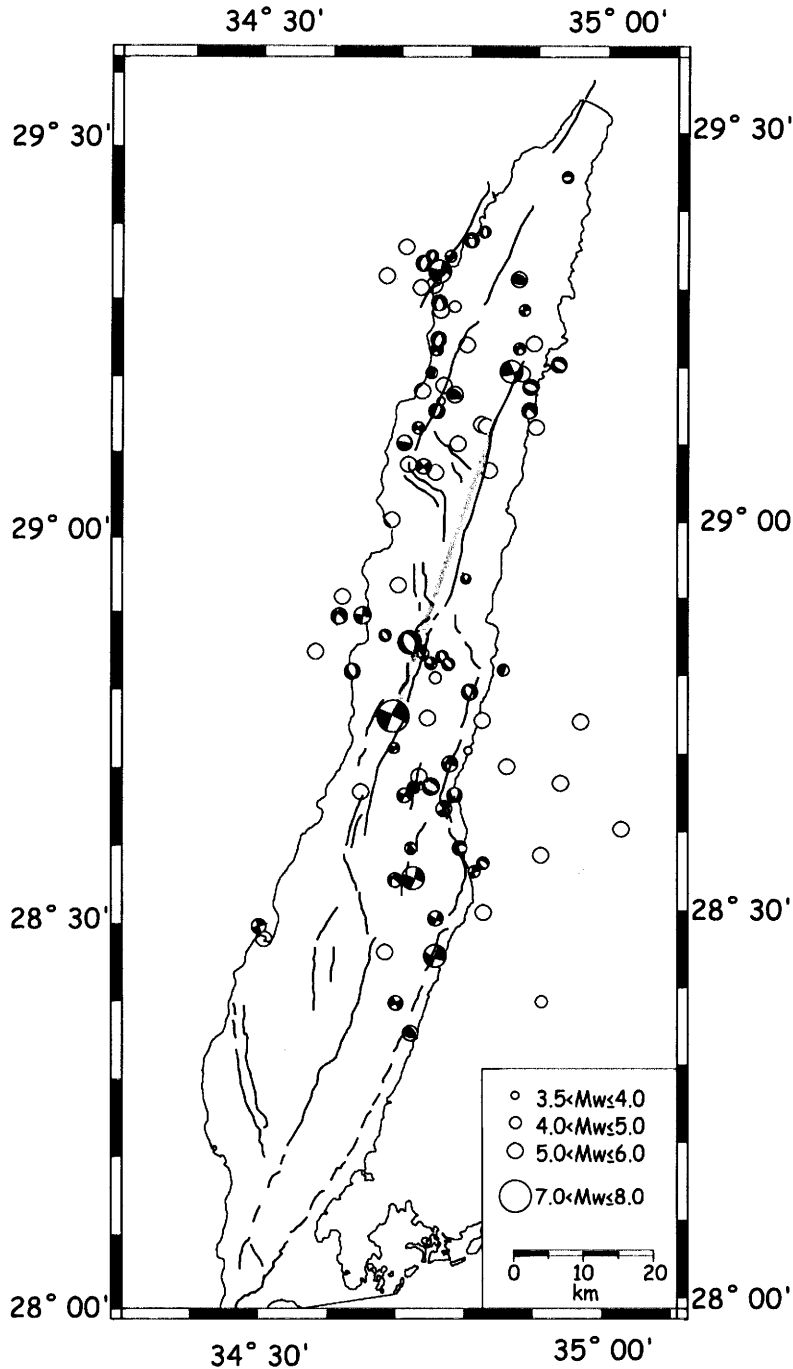


Figure 10. Distribution and source mechanisms of aftershocks that occurred during the 8 months following the Nuweiba earthquake.

zone of the same orientation at the northern end of the Aragonese basin, north of the epicentre (Fig. 10). These normal events are shallower (down to ~18 km) than the strike-slip aftershocks in the northern and southern clusters (approximately 25 km; Fig. 11a) and have downward-decreasing inclinations (Fig. 11b). They reflect a south-dipping normal cross fault, with a peak $M_w = 5.2$ event 86 days after the mainshock, which was activated by the Nuweiba earthquake.

6 DISCUSSION

Modelling of surface displacements in order to simulate interferometric SAR images based on mean static source parameters has been carried out frequently in recent years (e.g. Meyer *et al.* 1996; Baer *et al.* 1999; Feigl & Dupre 1999; Klinger *et al.* 1999; Wright *et al.* 1999; Delouis *et al.* 2000). These models have typically used solutions for the displacement field produced by finite dislocations

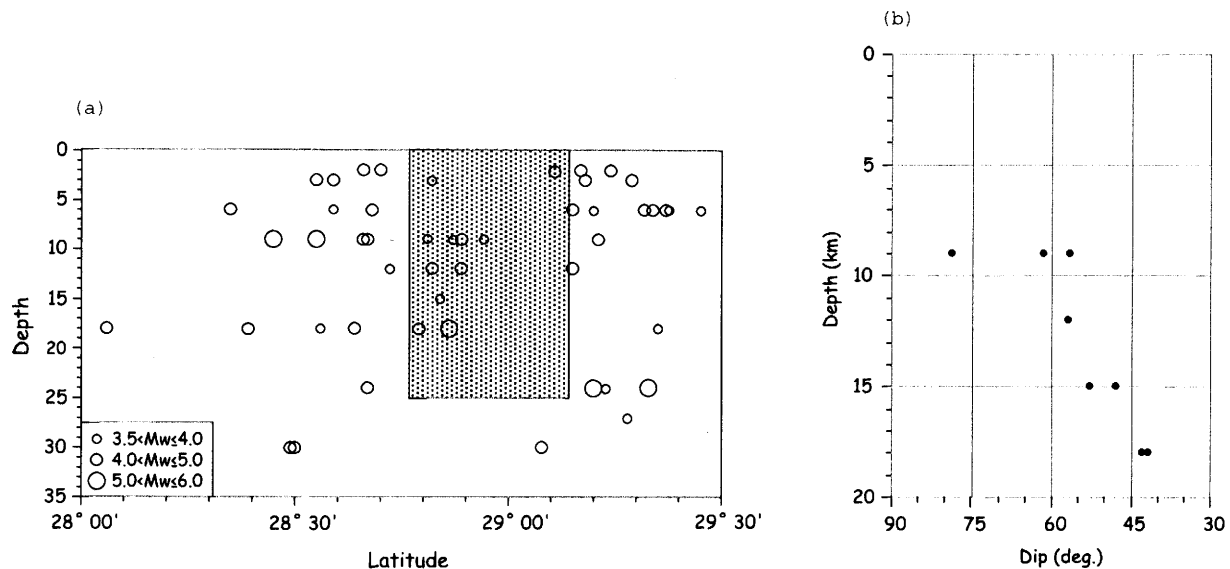


Figure 11. (a) Projection of aftershock hypocentres onto a gulf-parallel plane (mainshock section stippled), showing the difference in depth distribution between the step-over faults and the normal cross fault at the northern Aragonese basin (projected on the mainshock section). (b) Change of dip with depth for the north Aragonese basin normal mechanism aftershocks.

buried in an elastic half-space (e.g. Okada 1985), in which a uniform slip value is applied to the entire rupture surface and the effects of several faults can be superimposed but not solved in conjunction. While such models provide a useful far-field description of the displacement field and a reasonable general fit to InSAR images, they do not account for the near-field details of the slip distribution, fault geometry and the depth dependence of rigidity. As a result, their usage in estimating geodetic moments should be taken with caution. For example, in our first attempt at modelling the Nuweiba earthquake (Baer *et al.* 1999), a fringe rate inconsistency was first found between the InSAR and the simulated interferograms derived from a uniform dislocation model. Under such a model the only options were a deeper rupture, which is unreasonable given the magnitude of the earthquake ($M_w = 7.2$) and its well-constrained length, or significantly smaller uniform slip that would imply a far smaller seismic moment.

In this paper we adopt an approach in which the first priority is to model more realistic earthquake parameters, even if this means that a good fit to the observations is more difficult to achieve. Here, the complexity of the slip distribution, the geometry and the layered rigidity structure of the crust are taken into account using a discretized numerical model. The model uses the results of the body wave inversion of the Nuweiba earthquake as initial boundary conditions. Then, iterative modifications of the geometry and the distribution of slip and rake result in refinement of the static and kinematic source parameters. Our results show that the observed and simulated interferograms become consistent if the seismologically derived slip distribution is uniformly reduced by ~ 20 per cent and decaying slip gradients are imposed at the lateral edges and base of the slip patch. In that case the rupture reaches the bottom of the gulf, at an average water depth of 1 km. In addition, it is found that the surface area of the rupture patch was overestimated by the seismological solution by approximately 10–15 per cent. The best-fitting rupture model can be mostly enclosed in a 48×25 km² patch but its ‘surface’ (i.e. gulf floor) break is estimated to be less than 30 km.

These modifications result in a SAR-geodetic moment of 7×10^{19} N m, 10 per cent lower than the seismological estimate of Hofstetter *et al.* (2003). Our final best-fitting model is somewhat less successful in simulating the displacement at the southeast lobe of the rupture, possibly because we did not model the first subevent separately. Numerical modelling thus provides an improved means of constraining earthquake source parameters compared with dislocation models.

The occurrence of aftershocks outside the mainshock zone, or at least out of high slip/high moment areas, has been observed following many earthquakes (e.g. Das & Scholz 1981; Doser & Kanamori 1986; Hartzell & Heaton 1986; Mendoza & Hartzell 1988; Harris & Simpson 1992; King *et al.* 1994; Hodgkinson *et al.* 1996; Nalbant *et al.* 1996; Stein *et al.* 1997). It has been attributed, for example, to the increase in Coulomb shear stress induced by the mainshock onto neighbouring fault segments (Harris 1998, and references therein) and/or to transient pore pressure changes due to migration of pore fluids following a major earthquake (e.g. Nur & Booker 1972; Li *et al.* 1987). The absence of aftershocks along the main rupture was explained, e.g., by dilatancy hardening (Rudnicki & Chen 1988; Peltzer *et al.* 1998). In the case of the Nuweiba earthquake, while the appearance of normal cross-faulting within the mainshock near field (Fig. 10) may indicate a temporal decay of pore pressure, the continued absence of strike-slip mechanisms along the mainshock rupture segment at least 8 months into the post-seismic period suggests that the state of stress, and particularly the Coulomb stress change, was the dominant factor in determining the aftershock distribution and mechanisms.

The absence of strike-slip aftershocks along the mainshock rupture patch further indicates that the available fault-parallel Coulomb stress dropped below the frictional strength of the fault. At the same time, the lack of aftershocks below the coseismic rupture shows that there was no detectable stress transfer to the base of the seismogenic zone and transition to aseismic stable sliding, as suggested for the

1999 Izmit earthquake (Reilinger *et al.* 2000). On the other hand, the occurrence of oblique normal cross-faulting in the near field of the main rupture (Fig. 10) shows that the horizontal most compressive stress (S_{II}) dropped below the vertical stress (S_v) (i.e. the pre-seismic state of stress $\{S_{II} > S_v > S_h\}$ changed to $\{S_v > S_{II} > S_h\}$, where S_h is the horizontal least compressive stress), but there was no significant stress axis rotation as suggested for the Landers earthquake (Hill *et al.* 1993; Hauksson 1994). We therefore conclude that the shear stress drop of the Nuweiba earthquake was nearly, but not fully complete. Considering that the rupture occupied most of the non-overlapping extent of the Aragonese fault, the magnitude of the Nuweiba earthquake seems to be nearly the maximum possible on this, and by inference on other, similar segments of the DST. The normal cross-faulting aftershocks also show that under such stress modifications, basin subsidence directly follows large earthquakes along segmented strike-slip systems.

Our tectonic interpretation, which aligns the Nuweiba earthquake with the Aragonese fault, relies primarily on the near-field epicentre determination (Shamir 1996; Hofstetter *et al.* 2003). This epicentre is based on a very good azimuthal station coverage (an exceptional situation in the gulf of Elat/Aqaba) and, along with the rupture strike, is consistent with the only available fault map of the gulf (Hall & Ben-Avraham 1978; Ben-Avraham 1985). Klinger *et al.* (1999) proposed that the Nuweiba rupture consisted of three subevents, each breaking a distinct fault (Arnona, Aragonese and Elat), but this was based on qualitative arguments that are not supported by other independent data. These faults are nearly parallel, left stepping and approximately 10 km or more apart, which makes it unlikely (Harris & Day 1993) that the small first subevent could transfer the slip between the Arnona and Aragonese faults. As shown in this paper, and also implied by Klinger *et al.* (2000), the InSAR data strongly suggests that the rupture was confined to the Aragonese fault.

The relation of the Nuweiba earthquake to the 1983–1993 swarms is also not easily resolved due to the unsatisfactory station distribution throughout most of this period, leading to location errors that can reach the order of the distance between the faults. Thus, locating the swarms precisely on a specific fault or at the edge of the Nuweiba rupture (Klinger *et al.* 1999) seems speculative. In addition, the 1993 swarm is unlikely to have triggered the Nuweiba earthquake. As shown above, the Coulomb stress change induced on to the neighbouring faults was of the order of 1 bar or less, so it is likely that the stress changes due to the much smaller events of the 1983–1993 swarms were practically negligible in 1995.

Finally, we focus on the region northwest of the mainshock rupture, where the large $M_L = 5.6$ aftershock occurred (Fig. 10). This epicentre was determined to be onshore (Hofstetter *et al.* 2003), which is somewhat surprising due to the higher Coulomb stress change on the Elat fault, the immediate step-over fault near the Nuweiba rupture. The epicentre lies along the coast-parallel Muqbila fault (Fig. 2) that juxtaposes Precambrian igneous rocks against Holocene fan delta sediments and offsets Holocene sediments along the western coast of the gulf (Eyal 1973; Hildebrand *et al.* 1974; Bowman & Gerson 1986). The activation of the Muqbila fault by the Nuweiba earthquake is also indicated by InSAR observations of post-seismic deformation (Baer *et al.* 2001) and by a series of normal aftershocks apparently connecting it with the Elat fault (Fig. 10). This implies that the DST activity 'leaks' out of the gulf of Elat/Aqaba to the northwest. A similar conclusion was reached by Eyal (1973) based on observation of offset Holocene

sediments along the fault system branching out of the gulf to the NNW at an approximate latitude of $29^{\circ}30'$ (Fig. 2). If correct, this reflects a local modification of the plate boundary, a process that seems dominant over the direct Coulomb stress change induced by the Nuweiba earthquake. This would also have important implications for the seismic hazard in the cities of the northern gulf.

ACKNOWLEDGMENTS

We are grateful to Y. Eyal and two anonymous referees for fruitful comments and to H.-K. Thio for sharing results of the waveform inversion. This study was partially supported by grant no 98-00134 from the United States–Israel Binational Science Foundation (BSF), Jerusalem, Israel. ERS data were provided by the European Space Agency (ESA) under Category-1 project no 1058.

REFERENCES

- Alamri, A.M., 1991. Seismicity and aeromagnetic features of the gulf of Aqaba (Elat) region, *J. geophys. Res.*, **96**, 20 179–20 185.
- Allan, T.D., Charnock H. & Morelli, C., 1964. Magnetic, gravity and depth surveys in the Mediterranean and Red Sea, *Nature*, **204**, 1245.
- Baer, G., Sandwell, D., Williams, S., Bock, Y. & Shamir, G., 1999. Cosismic deformation associated with the November 1995, $M_w = 7.1$ Nuweiba earthquake, gulf of Elat/Aqaba, detected by synthetic aperture radar interferometry, *J. geophys. Res.*, **104**, 25 221–25 232.
- Baer, G., Shamir, G., Sandwell, D. & Bock, Y., 2000. Cosismic and postseismic deformation associated with the November 1995, $M_w = 7.1$ Nuweiba earthquake, gulf of Elat/Aqaba, analysed by Interferometric Synthetic Aperture Radar (InSAR) and elastic modeling, *27th General Assembly of the European Seismological Commission*, Lisbon, p. 37.
- Baer, G., Shamir, G., Sandwell, D. & Bock, Y., 2001. Crustal deformation during 6 yr spanning the $M_w = 7.2$ 1995 Nuweiba earthquake, analyzed by Interferometric Synthetic Aperture Radar, *Isr. J. Earth Sci.*, **50**, 9–22.
- Barazangi, M., Seber, D., Sandvol, E. & Vallve, M., 1996. Digital database development and seismic characterization and calibration for the Middle East and North Africa, *Department of Energy, USA*, PL-2222.
- Bartov, Y., 1974. A structural and paleogeographical study of the central Sinai faults and domes, *PhD thesis*, Hebrew University of Jerusalem.
- Bartov, Y., Steinitz, G., Eyal, M. & Eyal, Y., 1980. Sinistral movement along the gulf of Aqaba—its age and relation to the opening of the Red Sea, *Nature*, **285**, 220–221.
- Bechor, N., 1998. Measurements of current tectonic movements in the Sinai Subplate using GPS observations, *MSc thesis*, Tel Aviv University, Tel Aviv.
- Ben-Avraham, Z., 1985. Structural framework of the gulf of Elat/Aqaba, *J. geophys. Res.*, **90**, 703–726.
- Ben-Avraham, Z. & Tibor, G., 1993. The northern edge of the gulf of Elat, *Tectonophysics*, **226**, 319–331.
- Ben-Avraham, Z., Hanel, R. & Villinger, H., 1978. Heat flow through the Dead Sea rift, *Marine Geol.*, **28**, 253–269.
- Ben-Avraham, Z., Almagor, G. & Garfunkel, Z., 1979a. Sediments and structure of the gulf of Elat/Aqaba, *Sediment. Geol.*, **23**, 239–267.
- Ben-Avraham, Z., Garfunkel, Z., Almagor, G. & Hall, J.K., 1979b. Continental breakup by a leaky transform: the gulf of Elat/Aqaba, *Science*, **206**, 214–216.
- Bowman, D. & Gerson, R., 1986. Morphology of the latest Quaternary surface-faulting in the gulf of Elat region, eastern Sinai, *Tectonophysics*, **128**, 97–119.
- Das, S. & Scholz, C.H., 1981. Off-fault aftershock clusters caused by shear stress increase?, *Seis. Soc. Am. Bull.*, **71**, 1669–1675.
- Delouis, B., Lundgren, P., Salichon, J. & Giardini, D., 2000. Joint inversion of InSAR and teleseismic data for the slip history of the 1999 Izmit (Turkey) earthquake, *Geophys. Res. Lett.*, **27**, 3389–3392.

- Doser, D.I. & Kanamori, H., 1986. Depth of seismicity in the Imperial Valley region (1977–1983) and its relationship to heat flow, crustal structure and the October 15, 1979, earthquake, *J. geophys. Res.*, **91**, 675–688.
- Drake, C.L. & Girdler, R.W., 1964. A geophysical study of the Red Sea, *J.R. Astron. Soc.*, **8**, 473.
- Dreger, D. & Helmberger, D., 1993. Determination of source parameters at regional distances with three-component sparse network data, *J. geophys. Res.*, **98**, 8107–8125.
- El Isa, Z.H., Marghclani, H.M. & Bazzari, M.A., 1984. The gulf of Aqaba earthquake swarm of 1983 January–April, *GJRS*, **78**, 711–722.
- Eyal, Y., 1973. The tectonics of Shelomo and Yotam grabens, Elat, Israel, *Isr. J. Earth Sci.*, **22**, 165–184.
- Eyal, M., Eyal, Y., Bartov, Y. & Steinitz, G., 1981. The tectonic development of the western margin of the gulf of Elat/Aqaba rift, *Tectonophysics*, **80**, 39–66.
- Fattah, A.K., Hussain, H.M., Ibrahim, E.M. & Atta, A.S.A.E., 1997. Fault plane solutions of the 1993 and 1995 gulf of Aqaba earthquakes and their tectonic implications, *Ann. Geofis.*, **40**, 1555–1564.
- Feigin, G. & Shapira, A., 1994. A unified crustal model for calculating travel times of seismic waves across the Israel Seismic Network, *IPRG, Rep. Z1/567/79(107)*.
- Feigl, K.L. & Dupre, E., 1999. RINGCHN: a program to calculate displacement components from dislocations in an elastic half-space with applications for modeling geodetic measurements of crustal deformation, *Comp. Geosci.*, **25**, 695–704.
- Freund, R., Garfunkel, Z., Zak, I., Goldberg, M., Weissbrod, T. & Derin, B., 1970. The shear along the Dead Sea rift, *Phil. Trans. R. Soc. Lond.*, **A**, **267**, 105–127.
- Garfunkel, Z., Zak, I. & Freund, R., 1981. Active faulting in the Dead Sea rift, *Tectonophysics*, **80**, 1–26.
- Ginzburg, A., Makris, J., Fuchs, K., Prodehl, C., Kaminski, W. & Amitai, U., 1979. A seismic study of the crust and upper mantle of the Jordan–Dead Sea rift and their transition toward the Mediterranean Sea, *J. geophys. Res.*, **84**, 1569–1582.
- Gitterman, Y., Shapira, A. & Peled, U., 1996. Analysis of strong motion records of the 22.11.95 Nuweiba Earthquake and its aftershocks, *Annual Meeting of the Israel Geological Society*, pp. 33, Elat.
- Gomberg, J., Boelcler, N.M., Blanpied, M.L. & Bodin, P., 1998. Earthquake triggering by transient and static deformations, *J. geophys. Res.*, **103**, 24411–24426.
- Hall, J.K. & Ben-Avraham, Z., 1978. *Bathymetric Chart of the Gulf of Elat*, Geological Survey of Israel, Jerusalem.
- Harris, R.A., 1998. Introduction to special section: stress triggers, stress shadows and implications for seismic hazard, *J. geophys. Res.*, **103**, 24347–24358.
- Harris, R.A. & Day, S.M., 1993. Dynamics of fault interaction: parallel strike slip faults, *J. geophys. Res.*, **98**, 4461–4472.
- Harris, R.A. & Simpson, R.W., 1992. Changes in static stress on southern California faults after the 1992 Landers earthquake, *Nature*, **360**, 251–254.
- Hartzell, S.H. & Heaton, T.H., 1986. Rupture history of the 1984 Morgan Hill, California, earthquake from the inversion of strong motion records, *Bull. seism. Soc. Am.*, **76**, 649–674.
- Hatcher, R.D., Jr, Zietz, I., Regan, R.D. & Abu-Ajamich, M., 1981. Sinistral strike slip motion on the Dead Sea rift: confirmation from new magnetic data, *Geology*, **9**, 458–462.
- Hauksson, E., 1994. State of stress from focal mechanisms before and after the 1992 Landers earthquake sequence, *Bull. seism. Soc. Am.*, **84**, 917–934.
- Hildebrand, N., Shirav, M. & Freund, R., 1974. Structure of the Western margin of the gulf of Elat/Aqaba in the Wadi El Quseib–Wadi Haimur area, Sinai, *Isr. J. Earth Sci.*, **23**, 117–130.
- Hill, D.P. *et al.*, 1993. Seismicity remotely triggered by the magnitude 7.3 Landers, California, earthquake, *Science*, **260**, 1617–1623.
- Hodgkinson, K.M., Stein, R.S. & King, G.C.P., 1996. The 1954 Rainbow Mountain–Fairview Peak–Dixie Valley earthquakes: a triggered normal faulting sequence, *J. geophys. Res.*, **101**, 25459–25471.
- Hofstetter, A., Thio, H.K. & Shamir, G., 2003. Source mechanism of the 22/11/95 gulf of Aqaba Earthquake and its aftershock sequence, *J. Seism.*, **7**, 99–114.
- Joffe, S. & Garfunkel, Z., 1987. Plate kinematics of the circum Red Sea—a re-evaluation, *Tectonophysics*, **141**, 5–22.
- Kanamori, H. & Anderson, D.L., 1975. Theoretical basis of some empirical relations in seismology, *Bull. seism. Soc. Am.*, **65**, 1073–1095.
- Katzman, R., tenBrink, U.S. & Lin, J., 1995. Three-dimensional modeling of pull-apart basins: implications for the tectonics of the Dead Sea basin, *J. geophys. Res.*, **100**, 6295–6312.
- Kikuchi, M., 1995. Teleseismic analysis of the gulf of Aqaba, Egypt, earthquake of Nov. 22, 1995, *YCU, Seismology Note #49*.
- Kimata, F., Taleb, A., Murakami, H., Furukawa, N., Mahmoud, S., Khalil, H., Sakr, K.O. & Hamdy, A.M., 1997. The Aqaba earthquake of November 22, 1995, and co-seismic deformation in Sinai Peninsula, deduced from repeated GPS measurements, *Acta Geod. Geoph. Hung.*, **32**, 53–71.
- King, G.C.P., Stein, R.S. & Lin, J., 1994. Static stress changes and the triggering of earthquakes, *Bull. seism. Soc. Am.*, **84**, 935–953.
- Klinger, Y., Riviera, L., Haessler, H. & Maurin, J.-C., 1999. Active faulting in the gulf of Aqaba: new knowledge from the M_w 7.3 earthquake of 22 November 1995, *Bull. seism. Soc. Am.*, **89**, 1025–1036.
- Klinger, Y., Michel, R. & Avouac, J.-P., 2000. Cosismic deformation during the M_w 7.3 Aqaba earthquake (1995) from ERS-SAR interferometry, *Geophys. Res. Lett.*, **27**, 3651–3654.
- Li, V., Scalce, S.H. & Cao, T., 1987. Postseismic stress and pore pressure readjustment and aftershock distributions, *Tectonophysics*, **144**, 37–54.
- Mart, Y., 1982. Incipient spreading center in the gulf of Elat, *Earth planet. Sci. Lett.*, **60**, 117–126.
- Massonnet, D. & Feigl, K.L., 1998. Radar interferometry and its applications to changes in the Earth's surface, *Rev. Geophys.*, **36**, 441–500.
- Mendoza, C. & Hartzell, S.H., 1988. Aftershock patterns and mainshock faulting, *Bull. seism. Soc. Am.*, **78**, 1438–1449.
- Meyer, B. *et al.*, 1996. The 1995 Grevena (Northern Greece) earthquake: fault model constrained with tectonic observation and SAR interferometry, *Geophys. Res. Lett.*, **23**, 2677–2680.
- Nalbant, S.S., Barka, A.A. & Alptekin, O., 1996. Failure stress changes caused by the 1992 Erzincan earthquake ($M_s = 6.8$), *Geophys. Res. Lett.*, **23**, 1561–1564.
- Nur, A. & Booker, J.R., 1972. Aftershocks caused by pore fluid flow?, *Science*, **175**, 885–887.
- Okada, Y., 1985. Surface deformation due to shear and tensile faults in a half space, *Bull. seism. Soc. Am.*, **75**, 1135–1154.
- Peltzer, G., Rosen, P., Rogez, F. & Hudnut, K., 1996. Poroelastic rebound in fault step-overs caused by pore fluid flow, *Science*, **273**, 1202–1204.
- Peltzer, G., Rosen, P., Rogez, F. & Hudnut, K., 1998. Poroelastic rebound along the Landers 1992 earthquake surface rupture, *J. geophys. Res.*, **103**, 30131–30145.
- Pinar, A. & Turkelli, N., 1997. Source inversion of the 1993 and 1995 gulf of Aqaba earthquakes, *Tectonophysics*, **283**, 279–288.
- Quennell, A.M., 1959. Tectonics of the Dead Sea Rift, *20th Int. Geol. Cong.*, Mexico, pp. 385–405.
- Reasenber, P.A. & Oppenheimer, D., 1985. FPFIT, FPPLLOT and FPPAGE: Fortran computer programs for calculating and displaying earthquake fault-plane solutions, *US Geological Survey, Open-File Report 85-739*.
- Reilinger, R.E. *et al.*, 2000. Cosismic and Postseismic fault slip for the 17 August 1999, $M = 7.5$, Izmit, Turkey earthquake, *Science*, **289**, 1519–1524.
- Rudnicki, J.W. & Chen, C.H., 1988. Stabilization of rapid frictional slip on a weakening fault by dilatant hardening, *J. geophys. Res.*, **93**, 4745–4757.
- Shamir, G., 1996. The November 22, 1995, Nuweiba earthquake, gulf of Elat/Aqaba: mechanical analysis, *Geophysical Institute of Israel, Rep. 550/87/96(114)*.
- Shamir, G. & Shapira, A., 1994. Earthquake sequences in the gulf of Elat, *27th General Assembly of the International Association of Seismology and Physics of the Earth's Interior*, Wellington, New Zealand.

744 *G. Shamir, G. Baer and A. Hofstetter*

Stein, R.S., Barka, A.A. & Dietrich, J.H., 1997. Progressive failure on the North Anatolian fault since 1939, *Geophys. J. Int.*, **128**, 594–604.

tenBrink, U.S., Katzman, R. & Lin, J., 1996. Three-dimensional models of crustal deformation near strike-slip faults, *J. geophys. Res.*, **101**, 16 205–16 220.

Trevelyan, J., Adcy, R.A. & Niku, S.M., 1995. Adaptive and dynamic anal-

ysis using the boundary element method, *Proc. SAE Vehicle Structural Mechanics conference*, Troy, Michigan.

Wright, T.J., Parsons, B.E., Jackson, J.A., Haynes, M., Fielding, E.J., England, P.C. & Clark, P.J., 1999. Source parameters of the 1 October 1995 Dinar (Turkey) earthquake from SAR interferometry and seismic bodywave modeling, *Earth planet. Sci. Lett.*, **172**, 23–37.